Conditional $1/f^{\alpha}$ noise: From single molecules to macroscopic measurement

N. Leibovich and E. Barkai

Department of Physics, Institute of Nanotechnology and Advanced Materials, Bar-Ilan University, Ramat-Gan 5290002, Israel

(Received 23 March 2017; revised manuscript received 14 June 2017; published 19 September 2017)

We demonstrate that the measurement of $1/f^{\alpha}$ noise at the single molecule or nano-object limit is remarkably distinct from the macroscopic measurement over a large sample. The single-particle measurements yield a conditional time-dependent spectrum. However, the number of units fluctuating on the time scale of the experiment is increasing in such a way that the macroscopic measurements appear perfectly stationary. The single-particle power spectrum is a conditional spectrum, in the sense that we must make a distinction between idler and nonidler units on the time scale of the experiment. We demonstrate our results based on stochastic and deterministic models, in particular the well-known approach of superimposed Lorentzians, the blinking quantum dot model, and deterministic dynamics generated by a nonlinear mapping. Our results show that the $1/f^{\alpha}$ spectrum is inherently nonstationary even if the macroscopic measurement completely obscures the underlying time dependence of the phenomena.

DOI: 10.1103/PhysRevE.96.032132

I. INTRODUCTION

In many applications, a fluctuating signal $I(t)$ is analyzed in the frequency domain using the sample spectrum

$$S(\omega) = \frac{|I_t(\omega)|^2}{t} = \frac{1}{t}\left|\int_0^t I(t')\exp(-\imath\omega t')dt'\right|^2, \quad (1)$$

where the measurement time t is assumed to be long. The power spectrum of many processes exhibits $1/f^{\alpha}$ noise,

$$S(\omega) \propto \omega^{-\alpha}, \quad (2)$$

with $0.5 < \alpha < 1.5$. This behavior is practically universal as it is found in a wide range of systems ranging from electronic devices, geological data, blinking quantum dots, and currents in ion channels, to name only a few examples [1–11]. Such $1/f^{\alpha}$ fluctuations are found down to the lowest frequencies measured, which are of the order of $2\pi/t$, where t is the measurement time. For example, t is roughly an hour for blinking quantum dots [8], three months for careful measurements of voltage fluctuations in semiconductors [9], or years for geological data [10].

Many papers and reviews, with careful analysis of macroscopic data, propagate the idea that the $1/f^{\alpha}$ phenomenon is based on standard concepts of stationarity [2,4,5], "in the absence of overwhelming evidence to the contrary" [2]. This has a vast consequence, since stationarity implies the standard definition of the spectrum, and its connection to the underlying stationary correlation function through the Wiener-Khinchin theorem holds [12].

The $1/f^{\alpha}$ spectra, Eq. (2), are problematic because when $\alpha \geqslant 1$, the integral over the spectral density, which gives the total power of the system, $\int_{1/t}^{\infty}\omega^{-\alpha}d\omega$, diverges when the measurement time goes to infinity due to the low-frequency behavior. However, clearly for a bounded process the total power must be finite, $\int_0^{\infty} S(\omega)d\omega < \infty$ [12]. The demand for a finite total power and the measurements of $1/f^{\alpha}$ noise in a vast array of systems seem to contradict each other [1,2,4,5].

One way to resolve this low-frequency paradox is to assume that the underlying process is nonstationary [13–16]. Mandelbrot suggested that the $1/f^{\alpha}$ power spectrum *ages*, which means that $S_t(\omega) \propto \omega^{-2+\beta}t^{-1+\beta}$, so $\alpha = 2-\beta$ [13]. Importantly, here the spectrum depends on the measurement time t (see details below), and the total power remains finite, $\int_{1/t}^{\infty} S_t(\omega)d\omega = \text{const}$ [14,16]. The time-dependent amplitude of $S_t(\omega)$ provides a normalizable spectral density, therefore it should naturally appear in a bounded process. In this scenario, the spectrum is a density, as it should be, in the sense that $S_t(\omega)$ is normalizable [16]. Models of such nonstationary behavior are found in the theory of glasses [17,18], blinking quantum dots, analytically and experimentally [8,14], nanoscale electrodes [19], and interface fluctuations in the (1+1)-dimensional Kardar-Parisi-Zhang (KPZ) class, both experimentally and numerically, using liquid-crystal turbulence [20]. Thus one school of thought supports the idea that the sample spectrum exhibits nonstationary features of a particular kind [16,19,21–23]. However, others argue that while Mandelbrot's nonstationarity scenario is theoretically elegant, it is not a universal explanation since it is backed only by a few experiments [8,19,20].

Why, 50 years after Mandelbrot has pointed out the idea of an aged spectrum, is there only a small amount of experimental evidence for a nonstationary power spectrum? In particular, why do many measurements of $1/f^{\alpha}$ noise in condensed-matter physics seemingly support the stationarity scenario? The key issue is the difference between macroscopic and microscopic measurements. A macroscopic measurement contains many microscopic realizations. For example, consider a current $I(t)$ flowing through a disordered medium. The macroscopic system has many channels of current in it, distributed in a complicated way in the sample. The macroscopic measurement of the power spectrum corresponds to the total signal $I(t)$ generated in the sample, e.g., the spectrum of the total current. By microscopic measurements we mean local observations of individual units, e.g., the internal channels of current in the medium. Of course the signals from all those units, added together, yield the macroscopic measurement.

Following Mandelbrot [13], we consider *conditional* measurements, which are important in the context of measuring noise in the microscopic approach. We denote the currents of units in the sample with $I_j(t)$, where $j = 1,\ldots,N$ is the unit's index. The core of the concept is to separate the set

$\{I_j(t)\}_{j=1}^N$ into two subsets, one with the realizations $I_j(t)$ that appear stationary on the measurement time interval (this set is called B). The other set, the complementary one, contains all the other realizations (the set B^c). Of course, to distinguish between the two subsets one needs to be able to perform measurements one nano-object at a time, namely microscopic measurements, e.g., when one measures a local observation of current in one small junction in the system. Traditional spectral theory, based on the Wiener-Khinchin theorem, holds for the stationary realizations in subset B. For a single-particle measurement we consider a conditional measurement that is observed only from realizations that appear stationarity in the measurement time interval. Then we average over set B (i.e., averaging over the measured realizations set). Note that the size of set B depends on the measurement time; as we increase the measurement time, the number of realizations in B is changing. Hence, a conditional spectrum, averaged over set B, may depend on time, as we show in detail below.

Our goal in this paper is to show that there is a profound difference between measurements of $1/f^\alpha$ noise on the single-particle level if compared with macroscopic measurements (defined below). As we will show, on the microscopic level, where one conditionally measures single particles, the power spectrum ages. However, macroscopic measurements yield a time-independent spectrum. In that sense, the tension between the two conflicting approaches to $1/f^\alpha$ noise, i.e., the stationary versus the nonstationary communities, is reduced. As we show below, the aged spectrum is valid even for the most basic model of $1/f^\alpha$ noise, namely the distributed kinetic models for a variety of processes, e.g., the two-state model, the Ornstein-Uhlenbeck model, etc.

To demonstrate the broad validity of the main results, we consider two classes of models. We begin with the widely popular distributed kinetic approach. Here, at least in principle, if one measures in a long time interval, the processes are stationary. In the second part of the paper we consider a very different class of processes, which are inherently nonstationary. We investigate stochastic models of blinking quantum dots and a deterministic model of intermittency. While the two classes of models are vastly different, the main conclusion is the same: there is an essential difference between single-particle and macroscopic measurements.

II. MACROSCOPIC VERSUS SINGLE-PARTICLE MEASUREMENTS

Consider a large set of N independent processes $\{I_j(t')\}$ observed in the time interval $[0,t]$, where $j \in \{1,2,\ldots,N\}$ is the unit's label. The single-particle spectrum is given by the periodogram Eq. (1), i.e., $S_j(\omega,t) = t^{-1}|\int_0^t I_j(t')\exp(-i\omega t')dt'|^2$ when t is long. For a stationary process, this sample spectrum is given by the cosine Fourier transform of the autocorrelation function of the observable $I_j(t)$ via the Wiener-Khinchin theorem [12]. Additional smoothing of the sample spectrum is also routinely performed [24]; see also [14,25]. In single-particle measurements, one samples n_s trajectories, i.e., $I_j(t')$, where $j = 1,\ldots,n_s$, and then defines an average with respect to the measured processes, namely

$$\langle S_t(\omega)\rangle_{\rm sp} = \sum_{k=1}^{n_s} S_k(\omega,t)/n_s, \tag{3}$$

where $1 \ll n_s \ll N$. Here $\langle . \rangle_{\rm sp}$ stands for single-particle measurements with ensemble averaging over a subset with size n_s. For a macroscopic measurement, the spectrum of many independent processes, all measured in parallel, is

$$\mathcal{S}_t(\omega)_{\rm mac} = \sum_{j=1}^{N} S_j(\omega,t) \tag{4}$$

(see also Appendix E). Only if all the processes are statistically identical and stationary we find that the macroscopic measurement is simply related to the single-particle procedure via $\mathcal{S}(\omega)_{\rm mac} = N\langle S(\omega)\rangle_{\rm sp}$. Our goal is to show that this time-independent relation does not hold for models of $1/f^\alpha$ noise. This is related to the way experimentalists choose the subensemble of single-particle measurements, as we now demonstrate with a simple two-state model.

III. RANDOM TELEGRAPH SIGNAL

Consider a two-state telegraph process, where $I_j(t) = I_0$ or $I_j(t) = -I_0$ with sojourn times in each state, $\{\mathcal{T}_1^j, \mathcal{T}_2^j, \ldots\}$, that are exponentially distributed with mean τ_j. After each waiting time, the realization switches to the other state. For a long measurement time, the process is stationary and ergodic such that [26]

$$\langle I_j(t_0)I_j(t_0+t')\rangle = I_0^2\exp(-2t'/\tau_j), \tag{5}$$

hence, using the Wiener-Khinchin theorem, the spectrum is

$$S_j(\omega) = I_0^2\frac{4\tau_j}{4+\omega^2\tau_j^2}. \tag{6}$$

The value of τ_j varies from one molecule to the other. It is a quenched random variable in the sense that it is fixed for each process $I_j(t)$. This is a crude model for a single molecule in low-temperature glasses; see, e.g., [27,28].

Consider a set of N telegraph processes in which the characteristic time scale τ_j is varying from one molecule to another, with a common probability density function (PDF)

$$P(\tau) = \mathcal{N}\tau^{-\beta}, \tag{7}$$

with $0 < \beta < 1$. For such a distribution to be meaningful, we introduce an upper and a lower cutoff, $\tau \in [\tau_{\rm min},\tau_{\rm max}]$, thus the normalization constant is $\mathcal{N} = (1-\beta)/[(\tau_{\rm max})^{1-\beta} - (\tau_{\rm min})^{1-\beta}]$.

The model of superimposed Lorentzian-shaped spectra with heavy-tailed distributed characteristic time τ is considered one of the best known explanations to the $1/f^\alpha$ phenomena [1,2,5,29,30]. It was first developed nearly eight decades ago for vacuum tubes [30], and later in the middle of the 1950s for semiconductors [29]. See further discussion in Sec. VII.

Now assume that a realization j did not move at all on the time scale of the experiment, namely it is localized in its initial state during the entire measurement period, e.g., a unit with $\tau_j \gg t$. This noiseless unit does not contribute to the

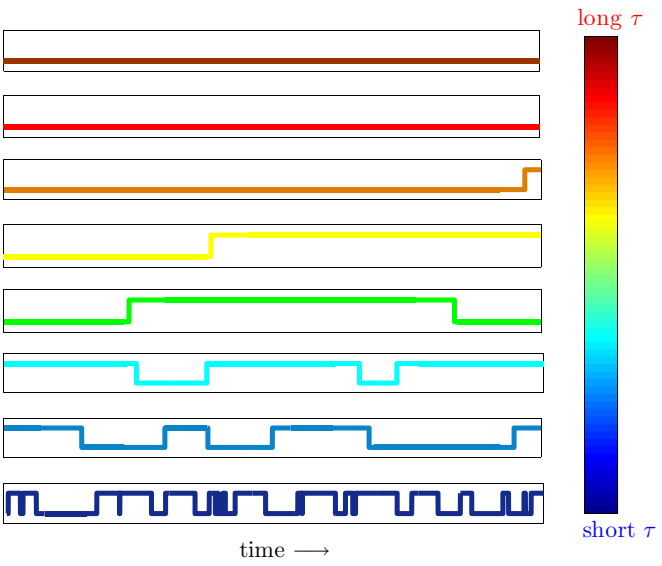

FIG. 1. An illustration for eight dichotomous Poisson processes with a characteristic time scale τ_j varying from one realization to another. The realization with the longest τ is given at the top (dark red), and then τ changes gradually where the shortest τ realization is given at the bottom (dark blue). It is clear that while changing the measurement time, the size of the set of moving realizations changes as well.

spectrum, since

$$S_t(\omega) = \frac{I_0^2}{t}\left|\int_0^t \exp(-\imath\omega t')dt'\right|^2 = I_0^2\frac{4\sin^2(\omega t/2)}{\omega^2 t}\bigg|_{\omega=2\pi n/t} = 0, \tag{8}$$

namely its sample spectrum vanishes at natural frequencies $\omega = 2\pi n/t$ when n is a positive integer. Since units with no activity are not detectable, i.e., they are noiseless, experimentalists measure only the active units' subensemble. Hence the single-particle spectrum is a conditional measurement.

The probability of a realization with a given relaxation time τ to move in the time interval $[0,t]$ is

$$\mathrm{P}_0^{\mathrm{mov}}(t|\tau) = 1 - \exp(-t/\tau), \tag{9}$$

which is equivalent to the probability that the first sojourn time in the initial state is longer than the measurement time, i.e., $\mathcal{T}_1 < t$; see Fig. 1.

Now we sample the spectrum of moving realizations only, thus we defined a conditional measurement of the spectrum. This protocol leaves us with a subset of $\{\tau_j\}$ of the moving objects, and the ensemble averaging is taken with respect to this subset. The normalized distribution of τ for the moving realization subset $\{\tau_j\}$ is $P(\tau)\mathrm{P}_0^{\mathrm{mov}}(t|\tau)\mathcal{N}_t$, where the time-dependent normalization constant is given by

$$\mathcal{N}_t^{-1} = \int_{\tau_{\min}}^{\tau_{\max}} \mathrm{P}_0^{\mathrm{mov}}(t|\tau)P(\tau)d\tau = \int_{\tau_{\min}}^{\tau_{\max}} (1-e^{-t/\tau})\frac{(1-\beta)\tau^{-\beta}}{\tau_{\max}^{1-\beta}-\tau_{\min}^{1-\beta}}d\tau \approx \Gamma(\beta)\left(\frac{t}{\tau_{\max}}\right)^{1-\beta}, \tag{10}$$

where the limit $\tau_{\min} \ll t \ll \tau_{\max}$ was taken. Averaging over the active particles' spectra yields

$$\langle S_t(\omega)\rangle_{\mathrm{sp}} \sim \mathcal{N}_t I_0^2 \int_{\tau_{\min}}^{\tau_{\max}} \frac{4\tau}{4+\omega^2\tau^2}\mathrm{P}_0^{\mathrm{mov}}(t|\tau)P(\tau)d\tau = \mathcal{N}_t I_0^2 \int_{\tau_{\min}}^{\tau_{\max}} \frac{4\tau}{4+\omega^2\tau^2}(1-e^{-t/\tau})\frac{(1-\beta)\tau^{-\beta}}{\tau_{\max}^{1-\beta}-\tau_{\min}^{1-\beta}}d\tau. \tag{11}$$

In the limit $\tau_{\min} \ll t \ll \tau_{\max}$ we approximate the integration interval to $[0,\infty)$. Then we find using MATHEMATICA

$$\int_0^\infty \frac{4\tau}{4+\omega^2\tau^2}(1-e^{-t/\tau})\tau^{-\beta}d\tau = -t^{2-\beta}\Gamma(\beta-2)\,{}_1F_2\left[1;\frac{3}{2}-\frac{\beta}{2},2-\frac{\beta}{2};-\frac{1}{16}t^2\omega^2\right] - \pi 2^{1-\beta}\omega^{\beta-2}\csc\left(\frac{\pi\beta}{2}\right)\left[\sec\left(\frac{\pi\beta}{2}\right)\cos\left(\frac{\pi\beta+t\omega}{2}\right)-1\right], \tag{12}$$

where ${}_1F_2[a;b_1,b_2;x]$ refers to the hypergeometric function. Then with the limit $\omega t \gg 1$ we obtain the single-particle spectrum, conditioned on measurements of the moving processes

$$\langle S_t(\omega)\rangle_{\mathrm{sp}} \simeq I_0^2 A_\beta \omega^{-2+\beta} t^{-1+\beta} \tag{13}$$

with $A_\beta = 2^{1-\beta}(1-\beta)\pi\csc(\frac{\pi\beta}{2})/\Gamma(\beta)$ for $0<\beta<1$. The conditional spectrum Eq. (13) thus provides the averaged spectra per contributing unit.

As was mentioned, from all N units only a fraction are contributing to the spectrum. The number of movers is $N_t \approx N \times \Gamma(\beta)(t/\tau_{\max})^{1-\beta}$ when $\tau_{\min} \ll t \ll \tau_{\max}$. The macroscopic measurement, therefore, is

$$\mathcal{S}(\omega)_{\mathrm{mac}} = N_t\langle S_t(\omega)\rangle_{\mathrm{sp}}. \tag{14}$$

The number of movers is increasing like $t^{1-\beta}$ while the spectrum $\langle S_t(\omega)\rangle_{\mathrm{sp}}$ [Eq. (13)] is decreasing as $t^{\beta-1}$, and we get from Eq. (14) a macroscopic spectrum

$$\mathcal{S}(\omega)_{\mathrm{mac}} \simeq N(I_0)^2 B_\beta \omega^{-2+\beta}(\tau_{\max})^{\beta-1} \tag{15}$$

with $B_\beta = 2^{1-\beta}(1-\beta)\pi\csc(\frac{\pi\beta}{2})$. This spectrum is found in a range of frequencies as low as $1/t$: there is no flattening effect, and the macroscopic measurement appears stationary since it is measurement-time-independent.

The macroscopic noise in Eq. (15) is proportional to N (as expected) multiplied by $(\tau_{\max})^{\beta-1}$, so unless one knows N (which includes also noiseless idlers), we cannot determine the upper cutoff time $\tau_{\max}$, which remains nondetectable as long as it is much larger than t. We comment that while both

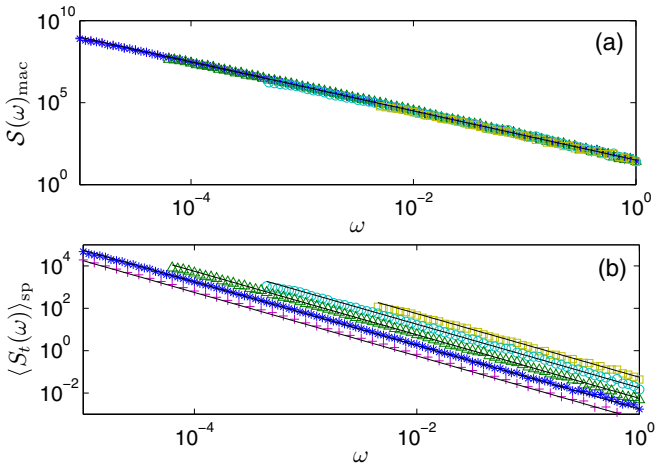

FIG. 2. Simulation results for the macroscopic spectrum [panel (a)] and the single-particle conditional spectrum [panel (b)]. We use $N = 10^5$ particles all following the two-state telegraph process with $I_0 = 1$ and relaxation times $\{\tau_j\}$ drawn from the fat-tailed PDF with $\beta = 1/2$, $\tau_{\rm min} = 1$, $\tau_{\rm max} = 10^8$, and $K = 0$. The spectrum was measured at measurement times; $t = 10^3$ (yellow squares), $t = 10^4$ (cyan circles), $t = 10^5$ (green triangles), $t = 10^6$ (blue stars), and $t = 10^7$ (pink crosses). The lines represent Eqs. (13) and (15). The macroscopic approach appears stationary while the conditional measurements reveal aged spectra.

N and $\tau_{\rm max}$ are nondetectable, $N(\tau_{\rm max})^{\beta-1}$ is a measurable quantity since the number of movers is $N_t \propto (t/\tilde{\tau}_N)^{1-\beta}$, where $\tilde{\tau}_N = \tau_{\rm max} N^{1/(\beta-1)}$ may, in principle, be measured.

In Fig. 2 we present the simulation results (symbols) and analytic results (solid lines) for the two-state telegraph noise processes. The characteristic time scale τ varies from one realization to another following the PDF in Eq. (7) with $\beta = 1/2$, $\tau_{\rm min} = 1$, and $\tau_{\rm max} = 10^8$. We show the aging effect for the single-particle spectrum: the spectrum is reduced as we increase the measurement time, and the whole spectrum is shifted to the red since the lowest measured frequency is of the order of $1/t$, in agreement with Eq. (13). Furthermore, finite-time simulation results show that the macroscopic approach appears stationary following Eq. (15).

It is rewarding that the superposition model, which is probably the most well-known model of $1/f^\alpha$ noise, shows aging if analyzed carefully. In contrast, when we measure the macroscopic power spectrum, an apparently stationary spectrum is found. This resolves the conflict between many empirical results, which found a time-independent $1/f^\alpha$ spectrum (e.g., [2,4,5]), and the nonstationary nature of $1/f^\alpha$ noise. Here, even though the macroscopic measured spectrum seems stationary, it still has a finite power; see further discussion in Sec. VII.

We note that the spectrum that is measured in the single-particle level, i.e., Eq. (13), depends neither on $\tau_{\rm min}$ nor $\tau_{\rm max}$. The reason is simple: the PDF of the relaxation times, $P(\tau) \sim \tau^{-\beta}$, where $0 < \beta < 1$, must have an upper bound for convergence, while a lower cutoff is not necessary and can go to zero. The measurement time t effectively serves as the upper cutoff. This means that the nature of the distribution, a heavy-tailed PDF, causes the measurement-time dependence of Eq. (13) while the spectrum is independent of the inherent cutoffs, $\tau_{\rm min}$ and $\tau_{\rm max}$, of the relaxation-time distribution. In Appendix A we discuss the cases in which the tail of $P(\tau)$ is "less heavy" in the sense that $P(\tau)\tau$ decays to a constant or to zero for large τ, i.e., $P(\tau) = O(1/\tau)$.

A. Condition of K transitions

So far we defined the single-molecule conditional measurement, based on the criterion of whether $I(t)$ jumped at least once from one level to another within the measurement time window $[0,t]$. This conditional measurement is not unique, and experimentally one may define other criteria; see further discussion in Appendix C. However, the main effect, an aging spectrum, is generally valid. For example, we define a process as measured if the number of jumps between the two states is more than K transitions, while a realization is not measured if the number of its transitions is less than or equal to K. In particular, the case $K = 0$ was considered in the previous section. Then the probability of a realization with a characteristic sojourn time τ to be conditionally measured is

$$\mathrm{P}_K^{\rm mov}(t|\tau) = 1 - e^{-t/\tau} \sum_{k=0}^{K} \frac{[t/\tau]^k}{k!} = 1 - \frac{\Gamma(1+K,t/\tau)}{K!} \tag{16}$$

and

$$\mathcal{N}_t^{-1} \approx \frac{\Gamma(\beta+K)(t/\tau_{\rm max})^{1-\beta}}{K!}, \tag{17}$$

where the limit $\tau_{\rm min} \ll t \ll \tau_{\rm max}$ is taken. Here we obtain the power spectrum for microscopic measurements,

$$\langle S_t(\omega)\rangle_{\rm sp} = \mathcal{N}_t I_0^2 \int_{\tau_{\rm min}}^{\tau_{\rm max}} \frac{4\tau}{4+\omega^2\tau^2} \times \left(1 - \frac{\Gamma(1+K,t/\tau)}{K!}\right) \frac{(1-\beta)\tau^{-\beta}}{\tau_{\rm max}^{1-\beta} - \tau_{\rm min}^{1-\beta}} d\tau, \tag{18}$$

and we recover the aging spectrum (13) with $A_\beta = K!2^{1-\beta}(1-\beta)\pi \csc(\frac{\pi a}{2})/\Gamma(\beta+K)$ for $0 < \beta < 1$, i.e.,

$$\langle S_t(\omega)\rangle_{\rm sp} \approx I_0^2 2^{1-\beta}(1-\beta)\pi \csc\left(\frac{\pi a}{2}\right) \frac{K!}{\Gamma(\beta+K)} t^{\beta-1}\omega^{\beta-2}; \tag{19}$$

see Fig. 3. A detailed derivation is given in Appendix B. As mentioned, here we take into consideration only units with more than K transitions, where $K \geqslant 1$. Those realizations are effectively units with τ_j shorter than t/K, hence the spectrum has a natural cutoff at $\omega_c \sim K/t$. This means that the spectrum flattens when $\omega < \omega_c$. This effect is unique to the conditional spectrum and is not found for the macroscopic measurement since the latter is not sensitive to the measurement condition and it follows Eq. (15) as before. The relation between the macroscopic spectrum and the conditional spectrum, Eq. (14), holds for frequencies higher than the crossover frequency ω_c (see also Appendix B).

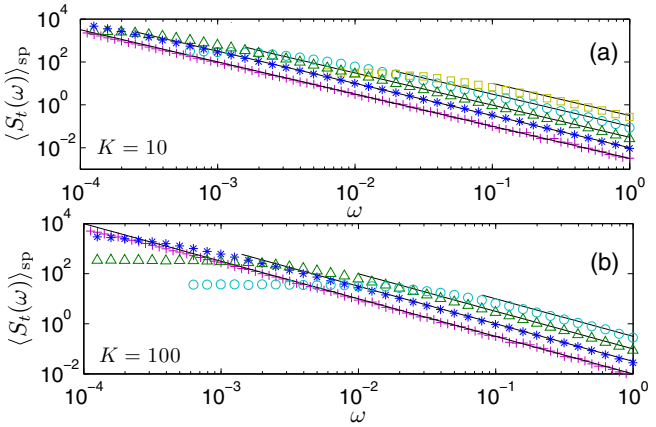

FIG. 3. Single-particle conditional spectrum, using the same parameters as in Fig. 2, however now altering the condition on the number of transitions, $K = 10$ [panel (a)] and $K = 100$ [panel (b)]. The aging effect is recovered, however now we have a cutoff frequency $\omega_c \sim K/t$ below which we observe a flattening effect of the spectrum. Solid lines represent Eq. (19).

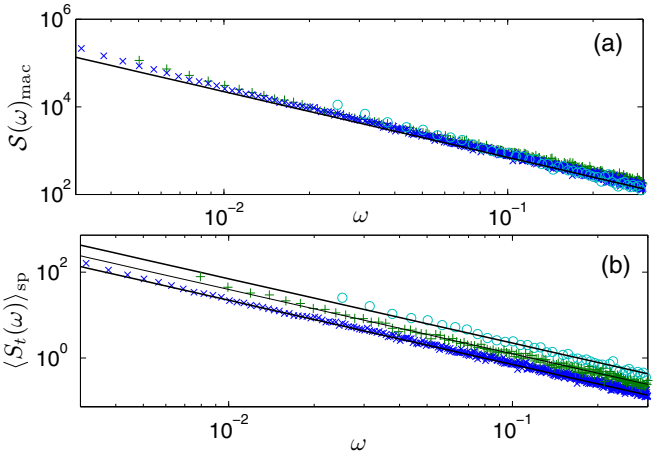

FIG. 4. Simulation results for the Ornstein-Uhlenbeck process with $N = 10^4$, $k_BT = 1$, and $m\omega_0^2 = 1$. The relaxation times are fat-tailed distributed with $\beta = 1/2$, $\tau_{\rm min} = 1$, and $\tau_{\rm max} = 10^6$. The measurement time of the spectrum was $t = 10^3$ (cyan circles), $t = 3162$ (green crosses), and $t = 10^4$ (blue stars). The analytic predictions Eqs. (23) are presented as solid lines. The conditional measurements of spectra reveal an aging effect, while the macroscopic approach obscures the nonstationarity.

IV. ORNSTEIN-UHLENBECK PROCESS

Our observation of the aging effect in the single-particle approach with conditional measurements is not limited to the two-state model. In the telegraph process in Sec. III, we defined two populations via the number of transitions between the states. In a real data set, the population can split into other categories, and in some cases the distinction between subsets of the populations is not obvious. For that reason, we consider N overdamped oscillators in contact with a thermal bath with temperature T. The process $I_j(t)$ is the position of the particle j, which is modeled with the Ornstein-Uhlenbeck process $\dot{I}_j = -(m\omega_0^2/\gamma_j)I_j + \eta(t)$ [31]. $\eta(t)$ is a white Gaussian noise with $\langle \eta(t)\eta(t')\rangle = 2D\delta(t-t')$, where $D = k_BT/\gamma$ satisfies the fluctuation-dissipation relation. The autocorrelation function of the jth particle is

$$\langle I_j(t_0+t')I_j(t')\rangle = \frac{k_BT}{m\omega_0^2}\exp(-t'/\tau_j) \tag{20}$$

with a relaxation time $\tau_j = \gamma_j/(m\omega_0^2)$, which is drawn from the mentioned PDF $P(\tau) \propto \tau^{-\beta}$ with $0 < \beta < 1$. For a particle j, when $t \gg \tau_j$, the spectrum of the process is Lorentzian since then it is effectively stationary,

$$S_j(\omega) = \frac{k_BT}{m\omega_0^2}\frac{2\tau_j}{1+\omega^2\tau_j^2}. \tag{21}$$

In the opposite limit, when $t \ll \tau_j$, this jth spectrum is far from Lorentzian and appears random due to the nonergodic behavior on these time scales (see also Appendix C). Unlike the two-state process, here we have two populations with distinct nontrivial spectra, i.e., we do not have noiseless units.

We distinguish between two populations: the first set contains realizations with $\tau_j < t$, which apparently exhibit Lorentzian spectra, and the second set contains realizations with $\tau_j \geqslant t$. The probability that a particle with a given relaxation time τ is measured is:

$$\mathrm{P}^{\rm mov}(t|\tau) = 1 - \Theta(\tau - t), \tag{22}$$

where $\Theta(x)$ is the Heaviside function. As in the previous model, the number of particles with Lorentzian spectra increases with time, $N_t \approx N(t/\tau_{\rm max})^{1-\beta}$. Therefore, the microscopic and the macroscopic measured spectra present a similar behavior to Eqs. (13) and (15) (respectively) with $A_\beta = B_\beta = (1-\beta)\pi\csc(\frac{\pi\beta}{2})$ and $I_0^2 = k_BT/(m\omega_0^2)$, namely we obtain

$$\begin{aligned}\langle S(\omega)\rangle_{\rm sp} &\approx \frac{k_BT}{m\omega_0^2}(1-\beta)\pi\csc\left(\frac{\pi\beta}{2}\right)t^{\beta-1}\omega^{\beta-2},\\ \mathcal{S}(\omega)_{\rm mac} &\approx N\frac{k_BT}{m\omega_0^2}(1-\beta)\pi\csc\left(\frac{\pi\beta}{2}\right)\tau_{\rm max}^{\beta-1}\omega^{\beta-2}.\end{aligned} \tag{23}$$

In Fig. 4, we present the simulation results where the power spectra of single particles (macroscopic samples) age (appear stationary). Optimization of single-molecule measurements and more advanced tools for distinguishing between populations are briefly discussed in Appendix C.

V. BLINKING QUANTUM DOT MODEL

So far we have considered two models in which the underlying kinetics is stationary in the sense that at least in principle, if we measure for an infinite time, the spectrum of each particle is Lorentzian. Here we consider a stochastic model of blinking quantum dots, which are nanocrystals that emit light with intensity $I(t)$ when interacting with a continuous-wave laser field. The stream of photons emitted blinks, and the process $I(t)$ exhibits on-off intermittency, with a power-law distribution of sojourn times in the on and off states. The power spectrum of single nanocrystals, measured *one at a time*, exhibits $1/f^{\alpha}$ fluctuations with clear nonstationary effects [8,32,33]. Here we focus on two unanswered questions: Do we observe the aging effect in

macroscopic measurements? How do $S_{\rm mac}(\omega)$ and $\langle S_t(\omega)\rangle_{\rm sp}$ differ?

To answer these questions, we define the following model. The signal, namely the light intensity, $I(t)$, takes two possible values, either $I(t) = I_0$ (state "on") or $I(t) = 0$ (state "off"). The blinking "on" $\leftrightarrow$ "off" sequence, for a single dot, is described by the set of "on" and "off" waiting times $(\mathcal{T}_1^{\rm on}, \mathcal{T}_2^{\rm off}, \dots)$. These sojourn times are statistically independent, identically distributed random variables with a common PDF $\psi(\tau) \propto \tau^{-(1+\beta)}$. This model is a variant of both the trap model for dynamics in glasses [17,34,35] and the velocity in the Lévy walk model [36]. In particular, [17] showed a nonstationary effect of the power spectrum of models of glassy dynamics, where the spectrum depends on the waiting time t_w defined below. In the blinking model, all the processes $I_j(t)$ are statistically identical, unlike the superposition model (Secs. III and IV), where each unit has its own time scale associated with it. In what follows, we assume $0 < \beta < 1$, hence the average waiting time diverges.

The N processes are initially, at time $t = 0$, in the state "on." We wait a long time t_w during which many transitions from "on" to "off" and vice versa take place. We then measure the spectrum by following the process in the time window $[t_w, t_w + t]$, so t is the measurement time. Also here we get two populations: a fraction of processes are jumping between the two states in the time window of observation (the movers), while other processes are stuck. In the single realization level, the idler's spectrum is zero. The movers are recorded in single-molecule experiments, and the conditional spectrum when $t \ll t_w$ reads [37]

$$\langle S_t(\omega)\rangle_{\rm sp} \simeq \frac{I_0^2}{2}\Gamma(2-\beta)\cos\left(\frac{\beta\pi}{2}\right) t^{\beta-1}\omega^{\beta-2}. \tag{24}$$

The spectrum ages with the measurement time t and is independent of the much longer waiting time t_w. To analyze the macroscopic measurement, we use a known formula for the probability to make at least one move in the time interval $[t_w, t_w + t]$ [26], thus the average number of movers in the measured interval is

$$N_t \simeq N\frac{\sin\pi\beta}{\pi(1-\beta)}\left(\frac{t}{t_w}\right)^{1-\beta} \tag{25}$$

when $t/t_w \ll 1$. Here as we increase t_w, leaving t fixed, we get fewer and fewer moving processes. This is expected since the longer t_w is, more and more processes get localized in one state in the observation window [38]. Using Eq. (14) we get a macroscopic spectrum that is measurement-time-independent,

$$\mathcal{S}(\omega)_{\rm mac} \sim I_0^2 N\frac{\beta\cos\left(\frac{\pi\beta}{2}\right)}{2\Gamma(1+\beta)}(t_w)^{\beta-1}\omega^{-2+\beta}. \tag{26}$$

Essentially this is similar to the superposition model, when we replace $\tau_{\rm max}$ with t_w, however the latter is a control parameter, together with the finite measurement time, in the experimental protocol. In Fig. 5, we show the simulation (symbols) and analytic (lines) results of both single-particle spectra and macroscopic ones, where the distinction is made visual.

To conclude, in Eq. (26) we see an aging spectrum in the spirit of the result of [17] in the sense that the spectrum depends on t_w. Equation (24) describes single-particle measurements of the spectrum, and of course there is no contradiction between the two.

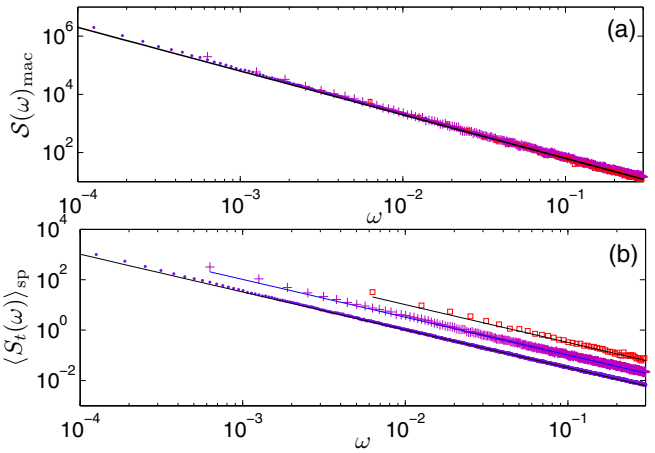

FIG. 5. Simulation results for the blinking-quantum-dot model with $\beta = 1/2$, $N = 10^4$, $I_0 = 1$, and $t_w = 10^6$ at measurement time $t = 10^3$ (red squares), $t = 10^4$ (pink crosses), and $t = 10^5$ (purple dots). The lines represent Eqs. (24) and (26). The conditional spectrum ages, unlike the macroscopic measurements that appear stationary.

VI. INTERMITTENT MAP

The essential difference between the method of measurements, i.e., the macroscopic and single-particle spectra, is not limited to stochastic processes. We have further extended the analysis to deterministic models, generating an intermittent signal from a Pomeau-Manneville type of map [39,40], and obtaining the spectra.

We consider a deterministic signal generated by the following map:

$$I_{t+1} = \mathcal{M}(I_t), \tag{27}$$

where t is a discrete time with unit time steps, and the map is given by

$$\mathcal{M}(I_t) = \begin{cases} I_t + (aI_t)^{1+1/\beta}, & 0 \leqslant I_t < \xi_1, \\ \frac{I_t-\xi_1}{\xi_2-\xi_1}, & \xi_1 \leqslant I_t \leqslant \xi_2, \\ I_t - [a(1-I_t)]^{1+1/\beta}, & \xi_2 < I_t \leqslant 1. \end{cases} \tag{28}$$

The signal is bounded, $0 < I_t < 1$, and I_t is a function of a discrete time t. This map has two unstable fixed points, at $I_t = 0$ and 1. The discontinuities ξ_1 and ξ_2 are determined by $\xi_1 + (a\xi_1)^{1+1/\beta} = 1$ and $\xi_2 - [a(1-\xi_2)]^{1+1/\beta} = 0$. The initial condition is uniformly distributed, and the process evolves via Eq. (28). Then we find for each realization its power spectrum corresponding to the signal recorded in the interval $[t_w, t_w + t]$.

The signal I_t exhibits a noisy on-off intermittency, due to the unstable fixed points. It is known [41,42] that the PDF of the sojourn times in the vicinity of each of the unstable fixed points is $\psi(\tau) \sim \tau^{-1-\beta}$, and that renewal theory discussed in Sec. V describes many properties of this deterministic process [41,42]. We distinguish between movers and idlers by the rule that if a signal crosses the threshold, e.g., $I^* = 1/2$, at least once in the time interval $[t_w, t_w + t]$, it is considered

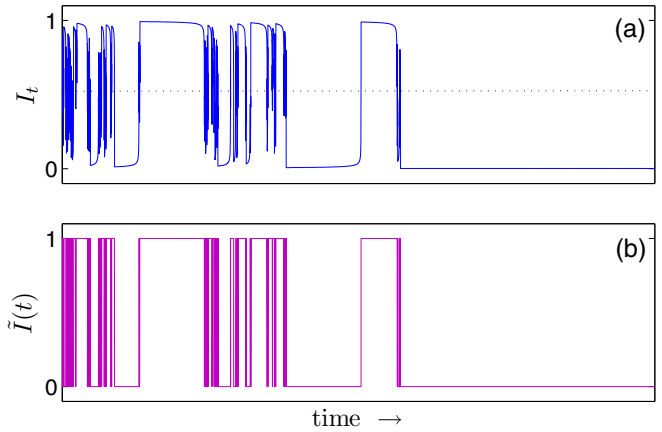

FIG. 6. The deterministic signal I_t [panel (a), blue] generated from the Pomeau-Manneville map (28) with $a = 1$ and $\beta = 1/2$. A realization is considered as a mover where I_t crosses the threshold $I^* = \frac{1}{2}$ (represented in a dashed line) at least once in the measurement-time period. The signal I_t is modeled with a two-state stochastic process $\tilde{I}(t)$ [panel (b), pink].

a mover (see Fig. 6). We record $N = 10^3$ realizations for averaging over the initial condition. In Fig. 7 we present the simulation results of the spectrum corresponding to the deterministic signals I_t. The macroscopic spectrum appears nonstationary while the conditional spectrum presents aging. This deterministic map is different, of course, if compared with the idealized stochastic on-off process discussed in the previous section; see Sec. V. Still the predictions of the simple stochastic two-state model Eqs. (24) and (26) presented as black lines in Fig. 7 seem to capture the main effects of aging.

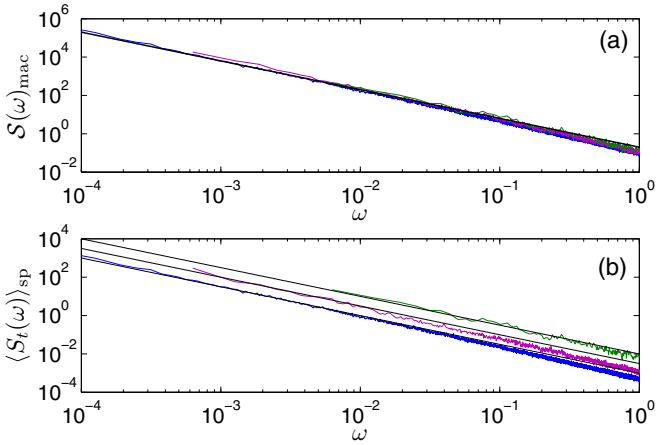

FIG. 7. A comparison between macroscopic (a) and single-particle measured spectrum (b) in the two-unstable-fixed points deterministic map (28). The waiting time is $t_w = 10^6$, $\beta = 0.5$, and $N = 10^3$ for three measurement times: $t = 10^3$ (green), $t = 10^4$ (pink), and $t = 10^5$ (blue). The black lines represent Eqs. (25) and (26).

VII. DISCUSSION

A. Convergence of the total power

The appearance of $1/f^{\alpha}$ noise with $\alpha \geqslant 1$ seems at first glance unphysical due to the divergences $\int_{1/t}^{\infty} \omega^{-\alpha} d\omega = \infty$ when $t \to \infty$. For an ergodic or a bounded process, the total power must be finite for the following reason: the total power when $t \to \infty$ is $\int_{1/t}^{\infty} S(\omega) d\omega \propto \int_0^t I(t')^2 dt'/t$ from Parseval's identity, therefore for a stationary ergodic process $\int_0^t I(t')^2 dt'/t = \langle I^2 \rangle$, which is finite. Furthermore, for a bounded process, i.e., $|I(t)| \leqslant I_{\rm max}$, regardless of whether it is ergodic or not, $\int_0^t I(t')^2 dt'/t \leqslant I_{\rm max}^2$, which is finite as well. This contradiction between the finite total power and the $1/f^{\alpha}$ measurements is sometimes called the "infrared catastrophe" or the "$1/f$ paradox," e.g., [11,13,14], as was mentioned in the Introduction.

The time-dependent $1/f^{\alpha}$ noise solves the contradiction between the vastly measured $1/f^{\alpha}$ noise and the convergence of the total power [16]. In this paper, we have found that the macroscopic measured spectrum appears stationary, i.e., it is time-independent. For example, consider the random telegraph model presented in Sec. III. This model is bounded, $I_{\rm max} = I_0$, and its macroscopic measured spectrum is time independent, $\mathcal{S}(\omega)_{\rm mac} \propto N(I_0)^2 \omega^{-2+\beta} \tau_{\rm max}^{-1+\beta}$, following Eq. (15). Nevertheless, it still poses a finite power since

$$\int_{1/t}^{\infty} \mathcal{S}(\omega)_{\rm mac} d\omega \propto N(I_0)^2 \int_{1/t}^{\infty} \omega^{-2+\beta} \tau_{\rm max}^{-1+\beta} d\omega$$
$$= N(I_0)^2 \left(\frac{t}{\tau_{\rm max}}\right)^{1-\beta} \leqslant N(I_0)^2 \qquad (29)$$

in the limit $t \ll \tau_{\rm max}$. In the opposite limit, $t \gg \tau_{\rm max}$, the spectrum bends at a frequency of order of $\tau_{\rm max}^{-1}$ and there is no low-frequency divergence anyway. A similar result, $\int_{1/t}^{\infty} d\omega\, \mathcal{S}(\omega)_{\rm mac} \leqslant N(I_0)^2$, is given for the quantum dot model (Sec. V) when we replace $\tau_{\rm max}$ with t_w, and $t \ll t_w$. Thus we conclude that for both microscopic and macroscopic measurements, the "low-frequency paradox" is solved.

B. Superposition model

We now discuss the problematic (in our opinion) analysis of $1/f^{\alpha}$ noise that we have found in the literature. As was mentioned, a widely used model that generates $1/f^{\alpha}$ noise, originally suggested in the late 1930s by Bernamont in the context of resistance fluctuations in thin films, is based on the superposition of many Lorentzian spectra [2,5,29,30]. This is also called the distributed kinetics approach to $1/f^{\alpha}$ noise, and it is probably the most well-known explanation of the phenomenon. As we consider in Secs. III and IV, the spectrum of the unit j is a measurement-time-independent Lorentzian

$$S_j(\omega) = \langle I^2 \rangle \frac{2\tau_j}{1 + \omega^2 (\tau_j)^2} \qquad (30)$$

with the time scale τ_j varying from one unit j to another with a common PDF,

$$P(\tau) = \mathcal{N} \tau^{-\beta}, \qquad (31)$$

with $0 < \beta < 1$ and $\tau_{\rm min} < \tau < \tau_{\rm max}$. Then the normalization constant is $\mathcal{N} = (1-\beta)[(\tau_{\rm max})^{1-\beta} - (\tau_{\rm min})^{1-\beta}]^{-1}$. By

averaging over the spectrum Eq. (30) we get an equation that serves as a starting point to many articles in the field [1,2,5],

$$\langle S(\omega)\rangle = \mathcal{N}\langle I^2\rangle \int_{\tau_{\min}}^{\tau_{\max}} \frac{2\tau}{1+\omega^2\tau^2}\tau^{-\beta}d\tau. \tag{32}$$

This formula must be used with care, since the spectrum Eq. (32) depends on $\tau_{\max}$, which is unphysical in the context of $1/f^\alpha$ fluctuations, for two reasons. It is clear that we must consider two cases, the first being when the measurement time t is shorter than $\tau_{\max}$. This is a typical situation, for example, in glassy systems in which $\tau_{\max}$ was estimated to be of the order of the universe's age [17,18]. In this case, Eq. (32) does not describe either macroscopic or microscopic spectra, since it depends on the cutoff time $\tau_{\max}$, which is not detectable on the time scale of the experiment. The second option, $t > \tau_{\max}$, is an experimental possibility, at least in principle, but if this holds we will *not* detect $1/f^\alpha$ noise at low frequencies [43]. In other words, at frequencies of the order of $1/t$, one observes a flat spectrum in disagreement with the very basic definition of the phenomenon. Indeed, many have searched for the bend down of $1/f^\alpha$ noise, mostly unsuccessfully; see, e.g., [9,10].

Therefore, the power spectrum Eq. (32) describes neither macroscopic nor microscopic measurements. On the one hand, Eq. (32) does not depend on the ensemble size N, and it cannot be considered as "macroscopic." On the other hand, Eq. (32) does not represent a microscopic measurement since it is independent of the measurement time t; see Eqs. (13), (19), (23), and (24).

C. A note on conditional measurements

Today, with advanced measurement techniques, one is able to record a signal from a single molecule or a nano-object; see, e.g., [44,45]. Therefore, the power spectrum of a microscopic unit, and further the conditional spectrum, becomes measurable. In the context of measurement of diffusion of single molecules in the live cell, conditional measurements are routinely performed. In this situation, one detects mixtures of spatially diffusing tracers and localized trapped particles, and the diffusivity is conditionally measured, i.e., averaged with respect to the moving subpopulation [38,46,47]. As we have shown here in the context of the $1/f^\alpha$ noise, these conditional measurements reveal an aging effect in basic models of $1/f^\alpha$ noise.

VIII. SUMMARY AND CONCLUSIONS

We have shown theoretically that an aging effect of the power spectrum is found in single-particle experiments, where measurements are conditional. However, the aging is totally obscured by the ensemble averaging, and it is not detected by macroscopic approaches. Our results are valid both for processes that exhibit stationarity at infinite time (e.g., random telegraph noise) and those that are essentially nonstationary (e.g., the quantum dot model). Certain aspects of the condition induce nonuniversal features, e.g., the cutoff $\omega_c = K/t$ [see Eq. (19)], while other features such as an aging spectrum are robust and in that sense universal. Our work is timely since today, with the advance of single molecule measurements, the distinction between the two types of measurements has become important. Thus conditional measurements, with their peculiar distinction from macroscopic ensemble averages, must be considered as a separate class of measurement protocol. We hope that this solves one of the oldest conflicts in nonequilibrium statistical mechanics. The nonstationary scenario for $1/f^\alpha$ noise, which was clearly overlooked in many reviews in the field, is a valid description of the most basic models of the field.

ACKNOWLEDGMENT

We thank the Israel Science Foundation for funding.

APPENDIX A: SUPERIMPOSED LORENTZIAN SPECTRA WITH OTHER RELAXATION-TIME PDF $P(\tau)$

1. Derivation for $\beta = 1$

$\beta = 1$ is an important special case, since it gives exactly $1/f$ noise. When $\beta = 1$ we find the normalization constant $\mathcal{N} = [\ln(\tau_{\max}) - \ln(\tau_{\min})]^{-1}$. Then the fraction of moving realizations is

$$\begin{aligned}\mathcal{N}_t^{-1} &= \int_{\tau_{\min}}^{\tau_{\max}} (1-e^{-t/\tau})\frac{\tau^{-1}}{\ln(\tau_{\max})-\ln(\tau_{\min})}d\tau \\ &\approx \frac{\ln(t/\tau_{\min})}{\ln(\tau_{\max}/\tau_{\min})},\end{aligned} \tag{A1}$$

when $\tau_{\min} \ll t \ll \tau_{\max}$. The single-particle spectrum, therefore, is given by

$$\begin{aligned}\langle S(\omega)\rangle_{\rm sp} &= I_0^2 \int_{\tau_{\min}}^{\tau_{\max}} \frac{4\tau}{4+\omega^2\tau^2}(1-e^{-t/\tau})\frac{\tau^{-1}}{\ln(t/\tau_{\min})}d\tau \\ &\approx \frac{I_0^2\pi}{\ln(t/\tau_{\min})\omega},\end{aligned} \tag{A2}$$

and the macroscopic spectra read

$$\mathcal{S}(\omega)_{\max} \approx \frac{N(I_0)^2\pi}{\ln(\tau_{\max}/\tau_{\min})\omega}. \tag{A3}$$

We conclude that when $\beta = 1$, the spectrum depends on both bounds—upper and lower—of the relaxation times.

2. Discussion about the case in which $1 < \beta < 2$ and other relaxation-time distributions

When $0 < \beta < 1$ we find that the low relaxation-time cutoff, $\tau_{\min}$, does not affect the asymptotic results. This, however, would not be the case in which $1 < \beta < 2$. We assume a fat-tailed relaxation-time distribution with $P(\tau) \approx [(\beta-1)/\tau_{\min}^{1-\beta}]\tau^{-\beta}$, where the limit $\tau_{\min} \ll \tau \ll \tau_{\max}$ is taken. The probability that a realization with a relaxation time τ moves in the measurement interval $[0,t]$ is $\mathrm{P}_0^{\rm mov}(t|\tau) = 1 - \exp(-t/\tau)$. Then the normalized distribution of the measured τ is $P(\tau)\mathrm{P}_0^{\rm mov}(t|\tau)\mathcal{N}_t$, where

$$\begin{aligned}\mathcal{N}_t^{-1} &= \int_{\tau_{\min}}^{\tau_{\max}} d\tau\, \mathrm{P}_0^{\rm mov}(t|\tau)P(\tau) \\ &\approx \int_{\tau_{\min}}^{\tau_{\max}} d\tau(1-e^{-t/\tau})\frac{\beta-1}{\tau_{\min}^{1-\beta}}\tau^{-\beta} \overset{\tau_{\min}\ll t}{\longrightarrow} 1.\end{aligned} \tag{A4}$$

That means that the fraction of the measured particles converges to 1, i.e., all particles are measured. Therefore, we obtain

$$\langle S(\omega)\rangle_{\rm sp} \approx I_0^2 2^{1-\beta}\pi \csc\left(\frac{\pi\beta}{2}\right)\tau_{\rm min}^{\beta-1}\omega^{\beta-2}, \qquad \text{(A5)}$$

which appears stationary. The intuitive explanation is the following. The relaxation times PDF $P(\tau)\propto\tau^{-\beta}$ decay rapidly at long τ, and the fraction of units with long relaxation times is almost zero. Then the contribution to the spectrum from realizations with long relaxation times does not affect the spectra, and a finite measurement time will not change the measured spectra.

A stationary conditional spectrum is also found when the relaxation-time distribution decays faster than $1/\tau$, i.e., when $P(\tau)=o(1/\tau)$, which means that $\lim_{\tau\to t^-}P(\tau)\tau\to 0$. For example, $P(\tau)$ follows a Gaussian distribution or decays exponentially.

APPENDIX B: CONDITION OF K TRANSITIONS

We consider a blinking process that is defined by a two-state signal switching between $I(t)=+I_0$ and $I(t)=-I_0$. The sojourn times in each state are independent identically exponentially distributed random variables with characteristic mean τ_j for the jth particle. Thus, for a given unit, we draw the random waiting time $\mathcal{T}_1^j$ from the mentioned exponential distribution; the unit is in state $+I_0$ in the interval $[0,\mathcal{T}_1^j)$. Then we generate $\mathcal{T}_2^j$ and renew the process by switching to state $-I_0$, and so on. Then for a realization j the process is defined by the array of random variables $\{\mathcal{T}_1^j,\mathcal{T}_2^j,\mathcal{T}_3^j,\ldots\}$. As mentioned in the text, for unit j the mean of the variables $\{\mathcal{T}^j\}$, τ_j, is fixed, and it varies from one unit to the other.

The stationary correlation function of realization j is

$$\langle I_j(t)I_j(t+t')\rangle = I_0^2\exp(-2t'/\tau_j), \qquad \text{(B1)}$$

where the relaxation time is τ_j. The corresponding spectrum is obtained from the Wiener-Khinchin theorem

$$S_j(\omega) = I_0^2\frac{4\tau_j}{4+\tau_j^2\omega^2}. \qquad \text{(B2)}$$

In our model, the mean sojourn times $\{\tau_j\}$ are identical independent distributed random variables with probability density function

$$P(\tau)=\mathcal{N}\tau^{-\beta}, \quad \tau_{\rm min}<\tau<\tau_{\rm max} \qquad \text{(B3)}$$

with normalization constant $\mathcal{N}=(1-\beta)[\tau_{\rm max}^{1-\beta}-\tau_{\rm min}^{1-\beta}]^{-1}$, where $0<\beta<1$.

The conditional microscopic measurement includes only realizations that exhibit more than K transitions in the time interval $[0,t]$. The probability of a given realization with mean waiting time τ to be measured is found using the Poisson distribution

$$\mathrm{P}_K^{\rm mov}(t|\tau) = 1-\sum_{k=0}^{K}\frac{e^{-t/\tau}[t/\tau]^k}{k!}, \qquad \text{(B4)}$$

where in the case $K=0$ we find $\mathrm{P}_0^{\rm mov}(t|\tau)=1-\exp[-t/\tau]$ as is given in Eq. (9). Then the normalization of the distribution of the active particles' relaxation times reads

$$\mathcal{N}_t^{-1} = \int_{\tau_{\rm min}}^{\tau_{\rm max}}\left(1-\sum_{k=0}^{K}\frac{e^{-t/\tau}(t/\tau)^k}{k!}\right)\frac{(1-\beta)}{\tau_{\rm max}^{1-\beta}-\tau_{\rm min}^{1-\beta}}\tau^{-\beta}d\tau = 1-\sum_{k=0}^{K}\frac{(1-\beta)t^k}{k!\left(\tau_{\rm max}^{1-\beta}-\tau_{\rm min}^{1-\beta}\right)}\int_{\tau_{\rm min}}^{\tau_{\rm max}}e^{-t/\tau}\tau^{-\beta-k}d\tau$$
$$= 1-\sum_{k=0}^{K}\frac{(1-\beta)t^{1-\beta}}{k!\left(\tau_{\rm max}^{1-\beta}-\tau_{\rm min}^{1-\beta}\right)}\left[-\Gamma\left(\beta+k-1,\frac{t}{\tau_{\rm min}}\right)+\Gamma\left(\beta+k-1,\frac{t}{\tau_{\rm max}}\right)\right]. \qquad \text{(B5)}$$

In the limit of $\tau_{\rm min}\ll t\ll\tau_{\rm max}$ we find

$$\mathcal{N}_t^{-1} \approx 1-\sum_{k=0}^{K}\frac{(1-\beta)t^{1-\beta}}{k!\tau_{\rm max}^{1-\beta}}\left[\Gamma(\beta+k-1)+\frac{t^{\beta+k-1}}{(1-\beta-k)\tau_{\rm max}^{\beta+k-1}}\right]$$
$$= 1-(1-\beta)\left(\frac{t}{\tau_{\rm max}}\right)^{1-\beta}\sum_{k=0}^{K}\frac{\Gamma(\beta+k-1)}{k!}-\sum_{k=0}^{K}\frac{(t/\tau_{\rm max})^k(1-\beta)}{k!(1-\beta-k)}$$
$$= 1+\frac{\Gamma(K+\beta)}{K!}\left(\frac{t}{\tau_{\rm max}}\right)^{1-\beta}-1+O\left(\frac{t}{\tau_{\rm max}}\right), \qquad \text{(B6)}$$

where we use the relation $\sum_{k=0}^{K}x^k/k!=e^x\Gamma(K+1,x)/K!$, and $\Gamma(a,z)=\int_z^{\infty}t^{a-1}e^{-t}dt$ is the incomplete Gamma function. Therefore, in the limit $t\ll\tau_{\rm max}$ we obtain

$$\mathcal{N}_t^{-1} \approx \frac{\Gamma(K+\beta)}{K!}\left(\frac{t}{\tau_{\rm max}}\right)^{1-\beta}. \qquad \text{(B7)}$$

When $K=0$ we recover $\mathcal{N}_t^{-1}\approx\Gamma(\beta)(t/\tau_{\rm max})^{1-\beta}$. Following Eq. (18), the conditional microscopic spectrum is thus

$$\langle S_t(\omega)\rangle_{\rm sp} \approx I_0^2\int_{\tau_{\rm min}}^{\tau_{\rm max}}\frac{4\tau}{4+\omega^2\tau^2}\left(1-\frac{\Gamma\left(1+K,\frac{t}{\tau}\right)}{K!}\right)\frac{(1-\beta)\tau^{-\beta}}{\mathcal{N}_t^{-1}\left(\tau_{\rm max}^{1-\beta}-\tau_{\rm min}^{1-\beta}\right)}d\tau. \qquad \text{(B8)}$$

Substitute $\mathcal{N}_t$ into that and expand the integration interval to $[0,\infty)$, where the limit $\tau_{\min} \ll t \ll \tau_{\max}$ is considered,

$$\langle S_t(\omega)\rangle_{\rm sp} \approx I_0^2 \int_0^\infty \frac{4\tau}{4+\omega^2\tau^2}\left(1-\frac{\Gamma\left(1+K,\frac{t}{\tau}\right)}{K!}\right)\frac{(1-\beta)K!}{\Gamma(K+\beta)t^{1-\beta}}\tau^{-\beta}d\tau. \tag{B9}$$

Integrating using MATHEMATICA gives

$$\begin{aligned}\langle S_t(\omega)\rangle_{\rm sp} \approx I_0^2\frac{(1-\beta)t}{\Gamma(K+\beta)}\Bigg\{&\frac{\Gamma(\beta+K-1)\,{}_2F_3\left[1,1-\frac{\beta}{2};2-\frac{\beta}{2},-\frac{\beta}{2}-\frac{K}{2}+1,-\frac{\beta}{2}-\frac{K}{2}+\frac{3}{2};-\frac{1}{16}(\omega t)^2\right]}{2-\beta}\\ &-\frac{\pi 2^{-\beta-K}(\omega t)^{\beta+K-1}\csc\left[\frac{1}{2}\pi(\beta+K-1)\right]{}_1F_2\left[\frac{K}{2}+\frac{1}{2};\frac{1}{2},\frac{K}{2}+\frac{3}{2};-\frac{1}{16}(\omega t)^2\right]}{K+1}\\ &+\frac{\pi 2^{-\beta-K-1}(\omega t)^{\beta+K}\sec\left[\frac{1}{2}\pi(\beta+K-1)\right]{}_1F_2\left[\frac{K}{2}+1;\frac{3}{2},\frac{K}{2}+2;-\frac{1}{16}(\omega t)^2\right]}{K+2}\Bigg\},\end{aligned} \tag{B10}$$

and expanding for $\omega t \gg 1$ yields

$$\langle S_t(\omega)\rangle_{\rm sp} \approx I_0^2 2^{1-\beta}(1-\beta)\pi\csc\left(\frac{\pi\beta}{2}\right)\frac{K!}{\Gamma(K+\beta)}t^{\beta-1}\omega^{\beta-2}. \tag{B11}$$

This result is given in Eq. (13) for $K=0$ with $A_\beta = 2^{1-\beta}(1-\beta)\pi\csc(\pi\beta/2)/\Gamma(\beta)$. More generally for $K>0$ we find $A_\beta = 2^{1-\beta}(1-\beta)\pi\csc(\pi\beta/2)\Gamma(K+1)/\Gamma(K+\beta)$. We use these results in Fig. 2 ($K=0$) and Fig. 3 ($K>0$).

Mathematically taking the opposite limit $\omega t \ll 1$ of Eq. (B10) gives, when $K \geqslant 1$,

$$\langle S(\omega t)\rangle_{\rm sp} \approx I_0^2\frac{t(1-\beta)}{(2-\beta)(K+\beta-1)}, \tag{B12}$$

which is frequency-independent, hence the spectrum bends from the $1/f^\alpha$ behavior; see Fig. 3. The crossover frequency ω_c is the frequency for which expression (B11) is equal to (B12) and is given by

$$\begin{aligned}\omega_c &\sim \frac{1}{t}\left(\frac{\Gamma(K+1)\pi\csc(\beta\pi/2)2^{1-\beta}(2-\beta)}{\Gamma(K+\beta-1)}\right)^{\frac{1}{2-\beta}}\\ &\underrightarrow[K\gg 1]{}\frac{2K}{t}[\Gamma(\beta/2)\Gamma(2-\beta/2)]^{\frac{1}{2-\beta}}.\end{aligned} \tag{B13}$$

We conclude that the conditional spectrum reveals a flattening of the $1/f^\alpha$ behavior at frequencies lower than ω_c; see the discussion and Fig. 3.

The macroscopic spectrum does not depend on the measurement condition and is given by

$$\mathcal{S}(\omega)_{\rm mac} \approx N(I_0)^2 2^{1-\beta}(1-\beta)\pi\csc\left(\frac{\pi\beta}{2}\right)(\tau_{\max})^{\beta-1}\omega^{\beta-2}. \tag{B14}$$

The relation between the macroscopic spectrum to the conditional spectrum, $\mathcal{S}(\omega)_{\max} = N_t\langle S_t(\omega)\rangle_{\rm sp}$, holds for frequencies higher than the crossover frequency ω_c.

APPENDIX C: DATA ANALYSIS IN THE ORNSTEIN-UHLENBECK PROCESS

In Sec. IV and in the simulation results presented in Fig. 4, we use the following question to separate between two populations: is the relaxation time shorter than the measurement time or not? This method has the advantage that the number of particles in the measured set is easily calculated. Then the microscopic spectra can be quantified, and a comparison between simulation results and Eq. (23) is presented in Fig. 4. However, in an experimental situation those relaxation times $\{\tau_j\}$ are *a priori* unknown. In the following, we suggest two other methods that are more practical to use in an experimental scenario.

One criterion to distinguish between the populations is based on whether the variance of $I(t)$ on the time scale of the measurement t is roughly given by the equipartition theorem. One may argue that particles that do not obey this rule have not reached equilibrium until the measurement time t. This thermal criterion, which may serve as a benchmark for conditioning the spectrum, is not unique.

A second procedure is based on the spectrum itself and hence is more detailed. Each individual realization's spectrum $S_j(\omega)$ is fitted to a Lorentzian shape $g_L(\omega)$ and to a spectrum of a Brownian particle (this is reasonable since the particles with large τ are freely diffusing) $g_B(\omega)$ with a fitting parameter $\hat{\tau}_j$,

$$g_L(\omega) = \frac{2\hat{\tau}_j^L}{1+\omega^2\left(\hat{\tau}_j^L\right)^2}, \quad g_B(\omega) = \left(\hat{\tau}_j^B\right)^{-1}\omega^{-2}. \tag{C1}$$

Confidence Interval: The first method for classification relies on the confidence interval. For each fitting model, g_L and g_B, we get the fitting parameter $\hat{\tau}_j^L$ corresponding to model g_L and $\hat{\tau}_j^B$ corresponding to g_B, and with 95% confidence in an interval (a_L,b_L) and (a_B,b_B), respectively,

General model :	$g_L(\omega)$	$g_B(\omega)$
Coefficients (with 95% confidence bounds) :	$\hat{\tau}_j^L$ (a_L,b_L)	$\hat{\tau}_j^B$ (a_B,b_B)

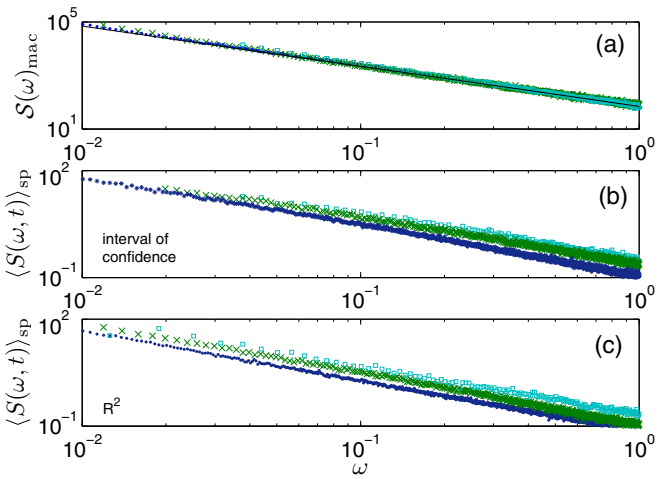

FIG. 8. The simulation results for the Ornstein-Uhlenbeck process. In panel (a) we present the macroscopic measured spectra at three measurement times: $t = 10^3$ (cyan squares), $t = 3162$ (green crosses), and $t = 10^4$ (blue dots). The black line represents the analytic prediction Eq. (23). In panels (b) and (c) we present the microscopic measured spectra, where we use the spectrum-based method for classification. The main result, the aging effect, is clearly visible in both classification methods.

We characterize the goodness of the Lorentzian fit by the width of the confidence interval $\mathrm{ci}_L = |b_L - a_L|/\hat{\tau}_j^L$, and similarly for the Brownian spectrum with $\mathrm{ci}_B = |b_B - a_B|/\hat{\tau}_j^B$. We classify a realization as Lorentzian when $\mathrm{ci}_L < \mathrm{ci}_B$ and as Brownian otherwise.

We note that such a classification method needs to be used with care since the regression hypothesis is not linear, and a nonconvex cost function may appear. In that case, the fitted parameter $\hat{\tau}$ may be affected by the initial searching point. Here, a deeper analysis is needed, and we leave it for a future publication.

Coefficient of Determination: A second method to determine the goodness of the fitting model is related to the coefficient of determination,

$$R^2 = 1 - \frac{\sum_{i=1}^{n}[S_j(\omega_i) - g(\omega_i)]^2}{\sum_{i=1}^{n}[S_j(\omega_i) - \overline{S_j}]^2}, \tag{C2}$$

where $\overline{S_j} = \sum_{i=1}^{n} S_j(\omega_i)/n$, and n is the number of observed frequencies. $R^2 \in [0,1]$, where R^2 is close to 1, means a reasonably good fitting. For a realization j we accept the Lorentzian assumption where $R_L^2 > R_B^2$ and we reject this assumption otherwise.

In Fig. 8 we present the simulation results for the macroscopic and microscopic spectra with the two classification methods suggested above. The macroscopic spectra, of course, do not depend on the measurement criteria and are left unchanged (upper panel). For the single-particle spectrum, both criteria reveal an aged spectrum (middle and lower panels), which is clearly visible in Fig. 8. The conclusion is that while the conditional spectrum is a rather general concept that depends on the choice of the experimentalists, the main conclusions in the text are still robust.

APPENDIX D: BLINKING QUANTUM DOT MODEL

We consider a two-state process, i.e., an "on" and "off" sequence, where the waiting times at each state are fat-tailed distributed with PDF $P(\tau) \sim \tau^{-1-\beta}$. The process switches to the other state after a sojourn time. Unlike the two-state model with exponential waiting times, here all units are statistically identical. However, none of them is stationary since $0 < \beta < 1$ implies the divergence of the mean sojourn time.

The macroscopic spectrum measured in a time interval $[t_w, t_w + t]$ for this two-state signal is [37]

$$\mathcal{S}(\omega)_{\rm mac} \approx N I_0^2 \frac{\cos(\pi\beta/2)}{2\Gamma(1+\beta)} \Lambda_\beta\left(\frac{t_w}{t}\right) t^{\beta-1}\omega^{\beta-2}, \tag{D1}$$

where the aging factor is $\Lambda_\beta(x) = (1+x)^\beta - x^\beta$. Therefore, in the limit $t_w \gg t$ we recover Eq. (26) in the text,

$$\mathcal{S}(\omega)_{\rm mac} \approx N I_0^2 \frac{\beta\cos(\pi\beta/2)}{2\Gamma(1+\beta)} t_w^{\beta-1}\omega^{\beta-2}. \tag{D2}$$

The probability of at least one transition in the measurement-time interval $[t_w, t_w + t]$ is [26]

$$P_0^{\rm mov}(t|t_w) = \frac{\sin(\pi\beta)}{\pi(1-\beta)}\left(\frac{t}{t_w}\right)^{1-\beta} {}_2F_1\left[1, 1-\beta; 2-\beta; -\frac{t}{t_w}\right] \underset{t\ll t_w}{\longrightarrow} \frac{\sin(\pi\beta)}{\pi(1-\beta)}\left(\frac{t}{t_w}\right)^{1-\beta}, \tag{D3}$$

and Eq. (24) in the main text is recovered.

APPENDIX E: PARALLEL MEASUREMENTS

We measured the spectrum for each realization, $S_j(\omega)$. These spectra are recorded simultaneously in parallel. Then the macroscopic spectrum is

$$\mathcal{S}(\omega)_{\rm mac} = \sum_{j=1}^{N} S_j(t,\omega). \tag{E1}$$

However, in some experimental cases, the macroscopic spectrum is measured via the macroscopic signal,

$$\tilde{\mathcal{S}}(\omega)_{\rm mac} = \frac{1}{t}\left|\int_0^t I(t')e^{\imath\omega t'}dt'\right|^2 = \frac{2}{t}\int_0^t\int_0^{t-t_1} I(t_1+\tau)I(t_1)\cos(\omega\tau)d\tau\, dt_1, \tag{E2}$$

where the macroscopic signal is $I(t) = \sum_j I_j(t)$. Therefore,

$$\tilde{\mathcal{S}}(\omega)_{\rm mac} = \frac{2}{t}\int_0^t\int_0^{t-t_1}\left(\sum_j I_j(t_1+\tau)\right)\left(\sum_{j'} I_{j'}(t_1)\right)\cos(\omega\tau)d\tau\, dt_1 = \frac{2}{t}\int_0^t\int_0^{t-t_1}\sum_j I_j(t_1+\tau)I_j(t_1)\cos(\omega\tau)d\tau\, dt_1$$

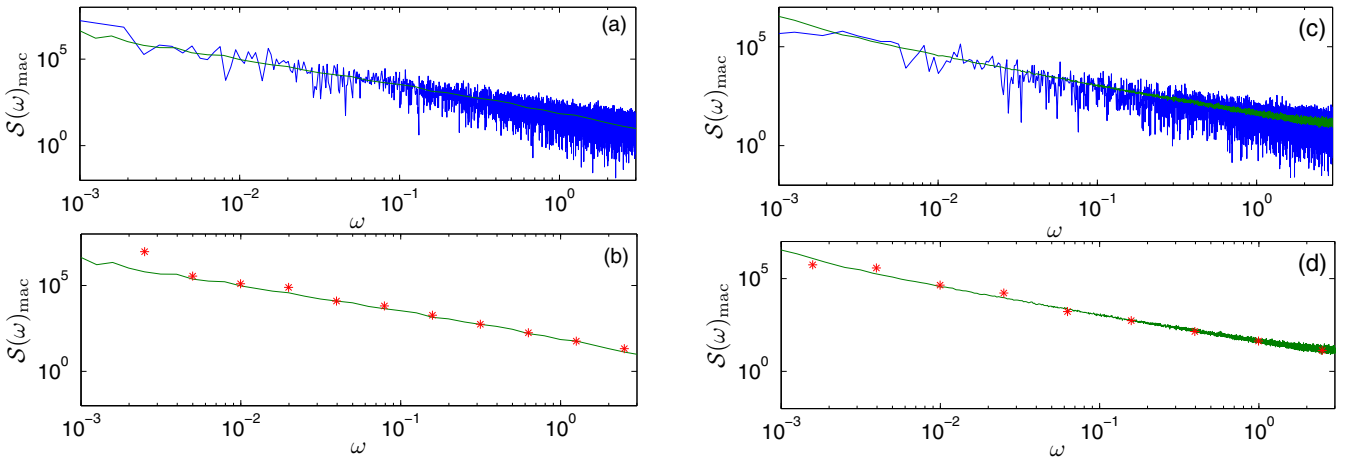

FIG. 9. (a),(c) Parallel measured power spectrum (green line) vs the total spectrum corresponds to the macroscopic signal (blue line) in two processes; the two-state random telegraph noise with $\beta = 1/2$, $\tau_{\rm min} = 1$, $\tau_{\rm max} = 10^5$, $N = 10^4$, and $t = 10^4$ [panels (a) and (b)] and the Ornstein-Uhlenbeck process with the same parameters [panels (c) and (d)]. (b),(d) The smoothed total spectrum (red stars) vs the paralleled measured spectrum (green line) shows that the parallel measurements provide a reasonable approximated measuring method.

$$+\frac{2}{t}\int_0^t\int_0^{t-t_1}\sum_j\sum_{j'\neq j} I_j(t_1+\tau)I_{j'}(t_1)\cos(\omega\tau)d\tau\,dt_1 =$$

$$=\sum_{j=1}^{N} S_j(t,\omega)+\frac{2}{t}\int_0^t\int_0^{t-t_1}\sum_{j=1}^{N}\sum_{j'\neq j} I_j(t_1+\tau)I_{j'}(t_1)\cos(\omega\tau)d\tau\,dt_1. \tag{E3}$$

Now, we claim that the second term on average is small, since the realizations are mutually independent with zero mean,

$$\left\langle\frac{2}{t}\int_0^t\int_0^{t-t_1}\sum_j\sum_{j'\neq j} I_j(t_1+\tau)I_{j'}(t_1)\cos(\omega\tau)d\tau\,dt_1\right\rangle = 0. \tag{E4}$$

In Fig. 9 we present the parallel measured spectrum versus the spectrum corresponding to the macroscopic signal in the random-telegraph-noise model and in the Ornstein-Uhlenbeck process. For the simulation we use $N = 10^4$ particles, $P(\tau) \propto \tau^{-1/2}$, where $\tau \in [1,10^5]$ and the measurement time is $t = 10^4$. The spectrum corresponding to the total macroscopic signal $I(t)$ is somewhat noisy (represented by a blue line), hence we smooth it with the moving average with logarithmic-width windows (red stars). The summation of the parallel measured spectra is represented by a green line. We conclude that the parallel measuring of the spectrum presents an agreement with the spectrum related to the total signal generated by the system.

APPENDIX F: SPECTRUM'S CONTRIBUTION FROM NEGLECTED PARTICLES

1. Two-state model

A particle is considered trapped when its physical quantity $I(t)$ is a constant during the measurement period. In such a case, the corresponding sample spectrum is

$$S_t(\omega) = \frac{I_0^2}{t}\left|\int_0^t \exp(-\imath\omega t')dt'\right|^2 = I_0^2\frac{4\sin^2(\omega t/2)}{\omega^2 t}. \tag{F1}$$

$S_t(\omega)$ vanishes at the natural frequencies, $\omega_n = 2\pi n/t$, for integer n.

2. Ornstein-Uhlenbeck process

In the two-state model, we consider a particle as trapped when $I(t) = \text{const}$ over the measurement interval. For the Ornstein-Uhlenbeck process, one needs to determine whether a given particle is trapped or not. Generally, a trapped particle is consider when the friction force is very strong. In that case, when τ is very small, the process is stationary and the spectrum is shown to be Lorentzian. In the other limit, for very weak friction force, i.e., long relaxation time, the particle is nearly diffusive, since it is not affected by the friction. The corresponding power spectrum is that of the Brownian noise, i.e., $S_j(\omega) \sim \omega^{-2}$, with a prefactor that is proportional to the diffusion constant $D = k_B T/m\omega_0^2\tau_j$.

3. Blinking quantum dot with additional white noise

As was mentioned, a constant signal in the time interval $(t_w, t_w + t)$ has no contribution to the measured spectrum in natural frequencies since

$$\left|\int_{t_w}^{t_w+t} e^{\imath\omega t'}dt'\right|^2 = \left[\frac{1-\cos(\omega t)}{\omega^2/2}\right]_{\omega=2\pi n/t} = 0. \tag{F2}$$

In that case, the trapped particles' spectrum is zero, and thus it cannot be detected. The addition of white (thermal) noise in the process, $\langle S(\omega)\rangle_{\rm th} = \sigma^2$, is reflected in the spectrum as

$$\mathcal{S}_{t_w}(\omega)^{\rm new}_{\rm mac} = \mathcal{S}_{t_w}(\omega)_{\rm mac} + N\langle S(\omega)\rangle_{\rm th}, \tag{F3}$$

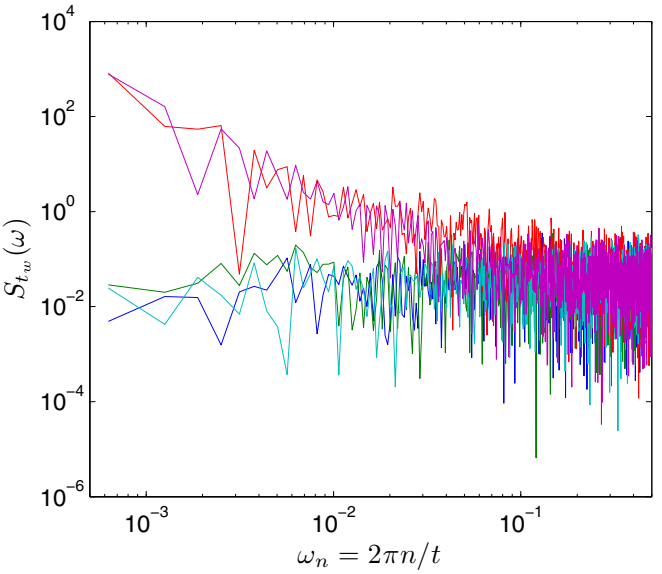

FIG. 10. The corresponding spectra of five blinking quantum dots. The two particles' spectra types are clearly observed; trapped particles exhibit white noise (green, blue, cyan) vs the nontrapped particles with $1/f^{\beta}$ noise (red, pink). Notice that differentiation between the two populations is manifest in sufficiently low frequencies, where in higher frequencies all the spectra are observed in a similar order of magnitude. For that reason, detecting the nonfrozen particles requires a long measurement time (corresponding to low frequencies).

where N is the number of molecules. The trapped particles generate white noise only, while the nontrapped particles exhibit $1/f^{\alpha}$ noise. Hence, one can distinguish between the two sets by their frequency-dependent spectra: constant spectra for the trapped particles versus power-law decay for the nontrapped ones. We illustrate this idea by presenting raw simulated data of five realizations of the blinking quantum dot model with additive white Gaussian noise with zero mean and variance $\sigma^2 = 0.05$, with $\alpha = 0.5$, $t_w = 10^5$, and $t = 10^4$ (see Fig. 10). The spectrum was calculated with the standard MATLAB fast Fourier transform function. In that case, we sort the particles into two types—trapped and nontrapped—without knowing whether the particle crossed the threshold or not. In fact, this concept of using the spectrum's frequency dependence may apply to a blinking quantum dot with strong white noise (i.e., large σ^2).

4. Deterministic intermittent map

Any measurement device has a minimum detection power, hence particles with lower power are undetectable. In the deterministic map model, we find that a particle whose signal I_t does not cross the threshold $I^* = 0.5$ exhibits very low power. A justification of this statement is illustrated in Fig. 11, where clearly the trapped particles exhibit very low power

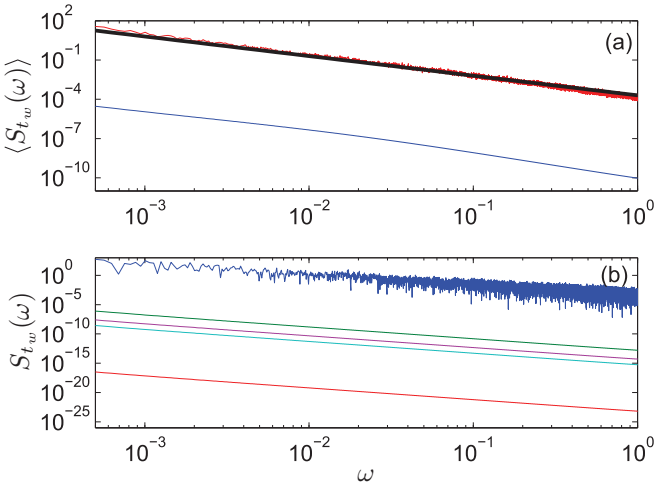

FIG. 11. The spectrum for the deterministic intermittent map with $\alpha = 0.5$, waiting time $t_w = 10^6$, and measurement time $t = 10^5$. In panel (a) we present the single-particle measurements (red line) and its $1/f^{\beta}$ noise prediction Eq. (24) (black curve). The blue line represents the averaged spectrum of the trapped particles (i.e., the particles that do not cross the threshold). In panel (b) five realizations of the spectrum are presented. The trapped particles (four bottom realizations) exhibit significantly low power related to the nontrapped particle (upper blue curve).

(related to the nontrapped particles). We present (bottom panel in Fig. 11) five realizations of the spectrum. In that case, where the minimal detection power is around 10^{-5}, realizations with lower power are undetectable.

5. Classification

Following Appendix C and the current appendix, we claim that distinguishing between two particles' populations—trapped and nontrapped—may not be trivial and is based on two main aspects. The first is the magnitude comparison of the spectra, where a trapped particle exhibits small amplitude in comparison to the nontrapped particles. In that case, the sensitivity threshold of the measurement device effectively determines which particle is detectable, i.e., if its corresponding power is smaller than a certain value, it cannot be detected. The second aspect of the differentiation between the particles' sets is the spectrum's frequency dependence. For example, we assume that each particle also has (thermal) white noise. In that case, a localized particle may produce power at the same order of magnitude as the nontrapped power. However, the trapped particle exhibits only the white noise, while a nontrapped particle provides $1/f^{\alpha}$ noise. The latter gives more power at lower frequencies while the white noise spectrum is simply a constant. Therefore, we find that two criteria used to distinguish between the two sets—the magnitude and the frequency dependence of the spectrum—both eventually present two sides of the same coin.

[1] A. Van Der Ziel, Physica **16**, 359 (1950).
[2] P. Dutta and P. Horn, Rev. Mod. Phys. **53**, 497 (1981).
[3] M. S. Keshner, Proc. IEEE **70**, 212 (1982).
[4] M. Weissman, Rev. Mod. Phys. **60**, 537 (1988).

[5] F. Hooge, T. Kleinpenning, and L. Vandamme, Rep. Prog. Phys. **44**, 479 (1981).
[6] L. Silvestri, L. Fronzoni, P. Grigolini, and P. Allegrini, Phys. Rev. Lett. **102**, 014502 (2009).
[7] J. Herault, F. Pétrélis, and S. Fauve, Europhys. Lett. **111**, 44002 (2015).
[8] S. Sadegh, E. Barkai, and D. Krapf, New J. Phys. **16**, 113054 (2014).
[9] M. Caloyannides, J. Appl. Phys. **45**, 307 (1974).
[10] B. B. Mandelbrot and J. R. Wallis, Water Res. **5**, 321 (1969).
[11] V. Solo, SIAM J. Appl. Math. **52**, 270 (1992).
[12] R. Kubo, M. Toda, and N. Hashitsume, *Statistical Physics II: Nonequilibrium Statistical Mechanics* (Springer, Berlin, 2012).
[13] B. B. Mandelbrot, IEEE Trans. Inf. Theor. **13**, 289 (1967).
[14] M. Niemann, H. Kantz, and E. Barkai, Phys. Rev. Lett. **110**, 140603 (2013).
[15] N. W. Watkins, in *Advances in Time Series Analysis and Forecasting: Selected Contributions from ITISE 2016*, edited by I. Rojas, H. Pomares, and O. Valenzuela (Springer International Publishing, Cham, 2017).
[16] N. Leibovich, A. Dechant, E. Lutz, and E. Barkai, Phys. Rev. E **94**, 052130 (2016).
[17] J.-P. Bouchaud, L. F. Cugliandolo, J. Kurchan, and M. Mezard, in *Spin-glasses and Random Fields*, edited by A. P. Young (World Scientific, Singapore, 1997).
[18] A. Crisanti and F. Ritort, J. Phys.: Math. Gen. **36**, R181 (2003).
[19] D. Krapf, Phys. Chem. Chem. Phys. **15**, 459 (2013).
[20] K. A. Takeuchi, J. Phys. A **50**, 264006 (2017).
[21] N. Leibovich and E. Barkai, Phys. Rev. Lett. **115**, 080602 (2015).
[22] A. Dechant and E. Lutz, Phys. Rev. Lett. **115**, 080603 (2015).
[23] M. A. Rodríguez, Phys. Rev. E **92**, 012112 (2015).
[24] W. H. Press, S. A. Teukolsky, W. T. Vetterling, and B. P. Flannery, *Numerical Recipes in Fortran 77: The Art of Scientific Computing* (Cambridge University Press, Cambridge, 1992).
[25] D. S. Dean, A. Iorio, E. Marinari, and G. Oshanin, Phys. Rev. E **94**, 032131 (2016).
[26] C. Godreche and J. Luck, J. Stat. Phys. **104**, 489 (2001).
[27] A.-M. Boiron, P. Tamarat, B. Lounis, R. Brown, and M. Orrit, Chem. Phys. **247**, 119 (1999).
[28] E. Geva and J. Skinner, J. Phys. Chem. B **101**, 8920 (1997).
[29] A. L. McWhorter, Sem. Surf. Phys., 207 (1957).
[30] J. Bernamont, Proc. Phys. Soc. **49**, 138 (1937).
[31] G. E. Uhlenbeck and L. S. Ornstein, Phys. Rev. **36**, 823 (1930).
[32] G. Margolin and E. Barkai, J. Stat. Phys. **122**, 137 (2006).
[33] S. Ferraro, M. Manzini, A. Masoero, and E. Scalas, Physica A **388**, 3991 (2009).
[34] E. Bertin and J. Bouchaud, J. Phys. A **35**, 3039 (2002).
[35] J.-P. Bouchaud, J. Phys. I **2**, 1705 (1992).
[36] V. Zaburdaev, S. Denisov, and J. Klafter, Rev. Mod. Phys. **87**, 483 (2015).
[37] M. Niemann, E. Barkai, and H. Kantz, Math. Model. Nat. Phenom. **11**, 191 (2016).
[38] J. H. P. Schulz, E. Barkai, and R. Metzler, Phys. Rev. X **4**, 011028 (2014).
[39] P. Manneville, J. Phys. **41**, 1235 (1980).
[40] Y. Pomeau and P. Manneville, Commun. Math. Phys. **74**, 189 (1980).
[41] T. Geisel and S. Thomae, Phys. Rev. Lett. **52**, 1936 (1984).
[42] G. Zumofen and J. Klafter, Phys. Rev. E **47**, 851 (1993).
[43] S. A. Diaz and M. Di Ventra, J. Comp. Elec. **14**, 203 (2015).
[44] F. D. Stefani, J. P. Hoogenboom, and E. Barkai, Phys. Today **62**(2), 34 (2009).
[45] R. Metzler, J.-H. Jeon, A. G. Cherstvy, and E. Barkai, Phys. Chem. Chem. Phys. **16**, 24128 (2014).
[46] I. Bronstein, Y. Israel, E. Kepten, S. Mai, Y. Shav-Tal, E. Barkai, and Y. Garini, Phys. Rev. Lett. **103**, 018102 (2009).
[47] A. G. Cherstvy and R. Metzler, Phys. Chem. Chem. Phys. **15**, 20220 (2013).